Available online at www.sciencedirect.com

SciVerse ScienceDirect

Ceramics International 39 (2013) S721–S727

CERAMICS INTERNATIONAL

www.elsevier.com/locate/ceramint

High-power properties and miniature ultrasonic motor of $(Sr,Ca)_2NaNb_5O_{15}$ piezoelectric ceramics

Yutaka Doshida[a,*], Hiroyuki Shimizu[a], Youichi Mizuno[a], Hideki Tamura[b]

[a]Taiyo Yuden Co., Ltd., 5607-2, Nakamuroda-machi, Takasaki-shi, Gunma 370-3347, Japan
[b]Tohoku Institute of Technology, Sendai 982-8577, Japan

Available online 1 November 2012

Abstract

We investigated the high-power properties of lead-free piezoelectric ceramics with $(Sr,Ca)_2NaNb_5O_{15}$ (SCNN), and clarified the properties of miniature cantilever-type ultrasonic motor of array-type multilayer piezoelectric ceramics of SCNN (SCNN–A–MLPC) as the lead-free-piezoelectric application. The jump phenomena of SCNN ceramics with constant-voltage driving produced mirror-reversed images relative to those of $Pb(Zr,Ti)O_3$-based (PZT) ceramics. The nonlinear behavior was caused by the hard-spring effect of SCNN ceramics which possess notable elastic properties among the piezoelectric materials. Under high vibration velocity with constant-motional-current driving, SCNN ceramics showed that the temperature rise was lower than that of PZT ceramics and the degradation of the quality factor was limited, resulting in a gradual increase in the equivalent mechanical resistance. SCNN ceramics have superior high-power properties. The cantilever-type ultrasonic motor was fabricated using SCNN–A–MLPC and the driving properties were evaluated. The output power of the motor increased linearly with increasing input power up to 110 mW without heat generation. The output power density was high in comparison with that of the commercialized motor of PZT ceramics. Furthermore, the refined motor with build in preload mechanism was fabricated and the driving properties were evaluated. The motor was able to rotate with 200 rpm and 40 μN m at 2.6 V_{p-p}. It appeared that the motors have a high potential as an environmental friendly piezoelectric device with excellent properties, reflecting the high-power properties of SCNN ceramics.

Keywords: C. Piezoelectric properties; C. Mechanical properties; E. Actuators

1. Introduction

There is a great demand for piezoelectric devices for use in the miniaturization of the mechanical components of mobile devices. The piezoelectric actuators have been partly put to practical use and many studies of ultrasonic motors have been carried out [1–4]. The piezoelectric actuators are almost always fabricated using $Pb(Zr,Ti)O_3$-based (PZT) ceramics. Under practical conditions; however, PZT ceramics easily experience a large strain and produce a notable degree of nonlinearity. The high-power properties occur as follows: the heat generation increases, the quality factor and certain performance characteristics of resonators deteriorate from the level they display under a small signal condition [5].

Recently, lead-free piezoelectric ceramics have been actively studied not only from the viewpoint of environmental conservation but also for the possibility of superior high-power characteristics [6–10]. The lead-free piezoelectric ceramics have also been applied to ultrasonic cleaners and miniature ultrasonic motors [10–14]. As a pioneer work, we succeeded in realizing an ultrasonic motor of lead-free piezoelectric ceramics by multilayer piezoelectric ceramics (MLPC) of $(Sr,Ca)_2NaNb_5O_{15}$ (SCNN) [11–13]. In particular, the motor using array-type MLPC of SCNN (SCNN–A–MLPC) was able to rotate by the voltage of a lithium-ion cell [12]. The driving properties were almost the same as those of a PZT motor under the low input power of 3 mW [12,13].

In this study, we investigated the high-power properties of SCNN ceramics by comparing with those of PZT ceramics, and clarified the properties of miniature cantilever-type ultrasonic motor with SCNN–A–MLPC

*Corresponding author. Tel.: +81 27 360 8307; fax: +81 27 360 8315.
E-mail address: ydoshida@jty.yuden.co.jp (Y. Doshida).

0272-8842/$ - see front matter © 2012 Elsevier Ltd and Techna Group S.r.l. All rights reserved.
http://dx.doi.org/10.1016/j.ceramint.2012.10.169

under high input power of 110 mW. Furthermore, the refined motor with build in preload mechanism was fabricated and the driving properties were evaluated. It appeared that the motor has high performance caused by the superior high-power properties of SCNN.

2. High-power properties

2.1. Sample preparation

SCNN powder was synthesized by a conventional solid-phase reaction [9]. Reagent-grade raw materials were weighed according to their compositions as $Sr_{1.9}Ca_{0.1}NaNb_5O_{15}$ and mixed by ball-milling with zirconia media and ethanol. After drying, the mixture was calcined and the power was pressed into disk. The disk was sintered at temperatures of 1200 °C. It was confirmed that their relative densities exceeded 97%, and X-ray diffraction analysis indicated a single-phase tungsten–bronze structure. An electrode was formed on the surface of the disk using the silver printing technique. Poling was performed by applying an electric field of 5 kV/mm for 15 min at 150 °C. The disk had a sample diameter of 8 mm and a thickness of 0.5 mm. The SCNN disk had an electromechanical coupling coefficient of $k_r=7\%$ and a mechanical quality factor of $Q_m=600$. For comparison, we prepared the hard PZT disk of $Pb(Zr,Ti)O_3$–$Pb(Ni,Nb)O_3$–$Pb(Zn,Nb)O_3$ with $k_r=60\%$ and $Q_m=1600$.

2.2. Measurement method

The high-power properties of the sample were investigated as a resonator in the first radial vibration mode using the continuous driving method in conjunction with a numerical equivalent model in a software-based system as reported in Ref. [15].

Fig. 1(a) shows a schematic of the sample being driven at the vibration velocity v, where V_D, I_f,θ_f, and T_r are the driving voltage, input current, its phase angle, and sample temperature, respectively. Fig. 1(b) shows the equivalent circuit configuration implemented in this study, where I_m, θ_m, C_d, R, L, and C are the motional current, its phase angle, the damped capacitance, the equivalent resistance, the equivalent inductance, and the equivalent capacitance, respectively. They also have the relationships $R=r/A^2$, $L=m/A^2$, $C=A^2/s$, and $I_m=Av$, where A, r, m, and s are

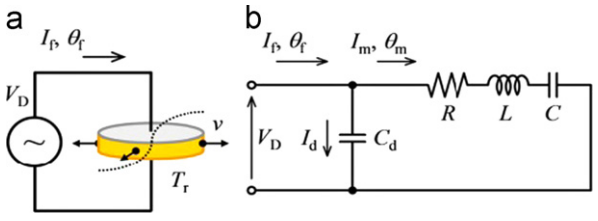

Fig. 1. (a) Schematic of sample setting for measurement, (b) equivalent circuit configuration implemented in this study.

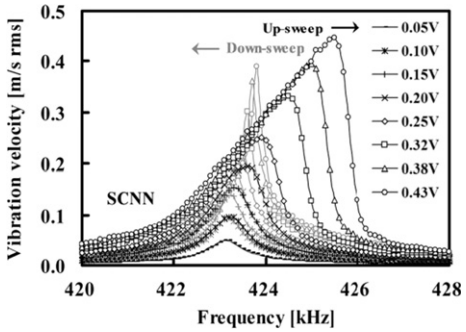

Fig. 2. Jump phenomena under constant-voltage driving for SCNN disk around resonance of first radial vibration mode.

the force factor, the equivalent mechanical resistance, the equivalent mass, and the equivalent stiffness, respectively.

r, m, and s have to be treated as functions of v and T_r for nonlinearity under high vibration velocity. The nonlinear behavior is observed as the jump phenomena, which are well known to be the hysteresis of the relationship between the vibration velocity and the frequency with constant voltage driving [15,16]. Fig. 2 shows the jump phenomena of the SCNN disk. The vibration velocity of the frequency up-sweep corresponded to that of the down-sweep under a low vibration velocity, however the hysteresis of vibration velocity from the frequency up-sweep and down-sweep could be clearly observed with an increase in the vibration velocity. The jump phenomena of the SCNN disk produced mirror-reversed images relative to those of PZT ceramics [15]. It is suggested that the nonlinear behavior of SCNN ceramics is induced by the hard-spring effect, in which the stiffness increases with an increase in the displacement. These mechanical characteristics are confirmed in the high-power properties below.

Therefore, the high-power properties have to be measured when the sample is driven by constants for v, T_r, and swept frequency, because the equivalent circuit becomes linearize. In this method, v was controlled by $|I_m|$, after T_f become a constant value in the steady state, the admittance circle was measured by changing θ_m. The admittance circle is written as

$$\left(G-\frac{1}{2R}\right)^2-(B-2\pi f_0 C_d)^2=\left(\frac{1}{2R}\right)^2, \quad (1)$$

with resonance frequency f_0, conductance G, and susceptance B. That is, it can provide the quality factor $Q = 1/(2\pi f_0 RC)$, r, m, and s at the driving level of high power properties.

2.3. High-power properties

Fig. 3 shows typical admittance circles for the SCNN disk. The admittance circle size was not dependent on the vibration velocity, however that of the hard PZT disk decreased with increasing vibration velocity as in the previous study [15].

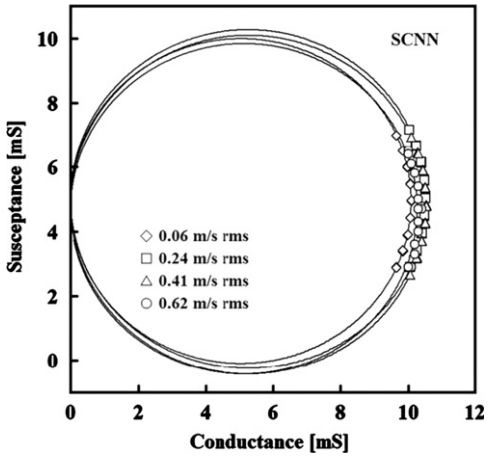

Fig. 3. Admittance circles under constant-vibration–velocity driving for the SCNN disk.

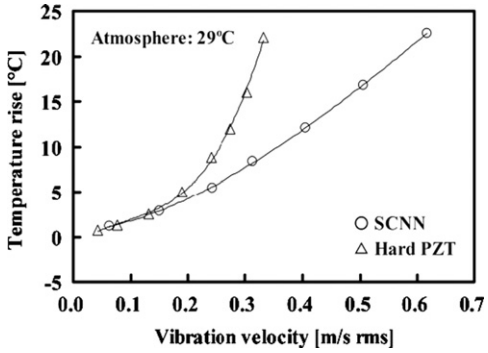

Fig. 4. Vibration velocity dependence of temperature rise of sample.

The measured temperature rises of the SCNN and PZT disks as a function of vibration velocity are shown in Fig. 4. The temperature rise of SCNN was lower than that of the hard PZT disk as reported in previous studies [8,15,16].

f_0 and s as a function of vibration velocity for the disks are shown in Fig. 5. f_0 of the SCNN disk increased and that of hard PZT decreased with increasing vibration velocity because of the vibration velocity dependence of s. This figure shows SCNN ceramics have a nonlinear hard-spring effect and hard PZT ceramics have a nonlinear soft-spring effect. The jump phenomena of the SCNN disk was caused by the nonlinear hard-spring effect. SCNN ceramics possess notable elastic properties among the piezoelectric ceramics. We are currently investigating the cause of nonlinear behavior.

Fig. 6 shows the vibration velocity dependence of Q and r for the SCNN disk and the hard PZT disk. Q of SCNN gradually increased and decreased with an increase in vibration velocity, with a broad peak. This appears to be a unique behavior. On the other hand, Q of hard PZT was over 1000 with low vibration velocity. However the Q drastically decreased with increasing vibration velocity and was lower than that of SCNN.

The tendencies of r corresponded to those of the inverse of Q in Fig. 6. The degradation of Q with increasing

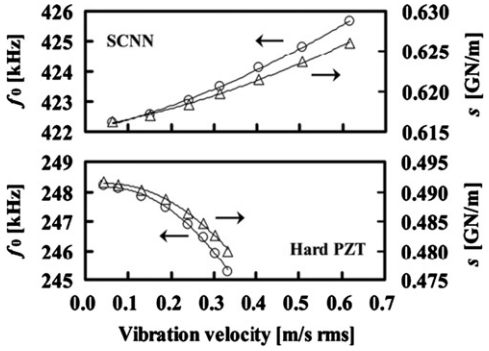

Fig. 5. Vibration velocity dependence of f_0 and s.

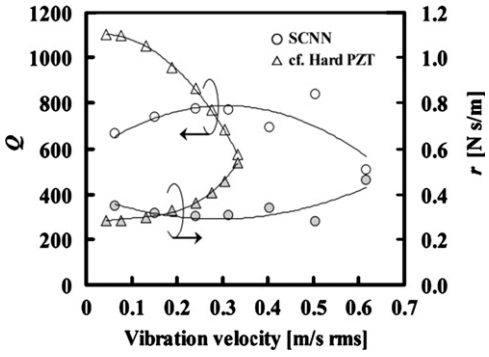

Fig. 6. Vibration velocity dependence of Q and r.

vibration velocity for SCNN ceramics was thus limited, resulting in a gradual increase in the r. In contrast, it was easy to degrade Q of hard PZT ceramics by drastically increasing r. It was clarified that SCNN ceramics have superior high-power properties in contrast to those of hard PZT ceramics.

3. Miniature ultrasonic motor properties

3.1. Motor design

The structure of stator vibrator is shown in Fig. 7 [11–13]. SCNN–A–MLPC integrated four pieces of MLPC arrayed in a 2×2 matrix and fabricated by applying multilayer ceramic capacitor technology. It had 40 active piezoelectric layers, the thickness of one layer of 18 μm because of the enhancing of piezoelectric properties. By the thickness vibration of two pairs of MLPC arranged diagonally in SCNN–A–MLPC, the stator vibrator is oscillated as the first-bending-vibration-mode rotation of the cantilever-type actuator in which its construction is very simple and enhanced displacement can easily be realized. The rotation direction can be changed by adjusting the phase difference between the voltages applied to each MLPC in A–MLPC.

Fig. 8 shows the motor with the stator vibrator. The rotor can be fixed in the rotation axis and rotated in the reverse direction with respect to the mode rotation of the vibrator by the friction force between the rotor side surface and the circumference of the vamplate of the vibrator.

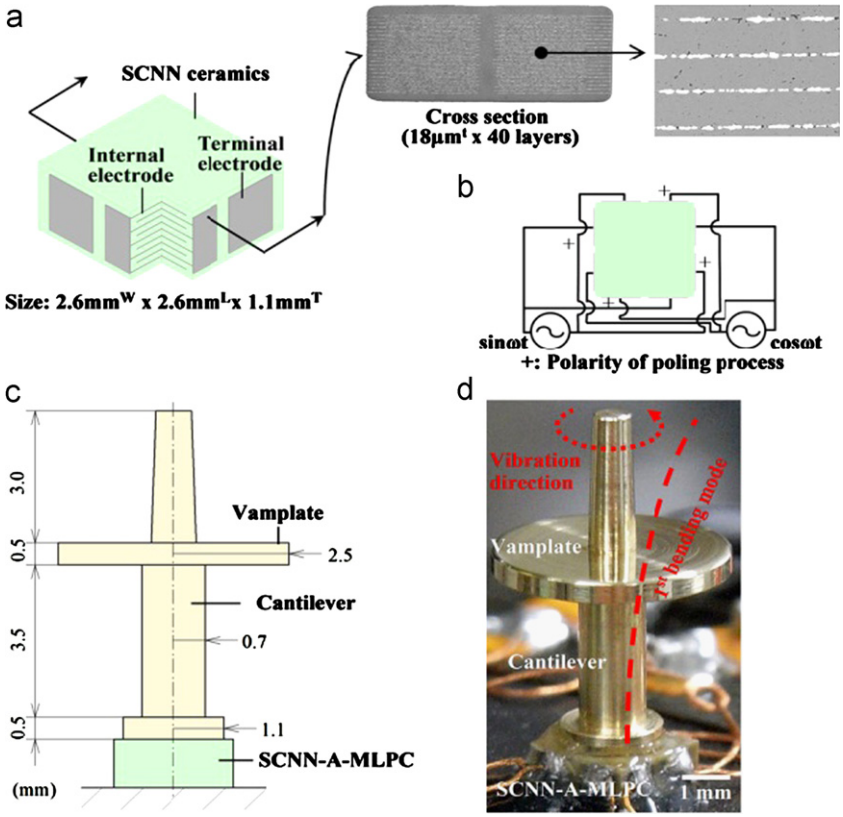

Fig. 7. Structure of stator vibrator using SCNN–A–MLPC: (a) overview and SEM image of cross section for A–MLPC, (b) wire diagram, (c) side view of stator vibrator, and (d) picture of stator vibrator.

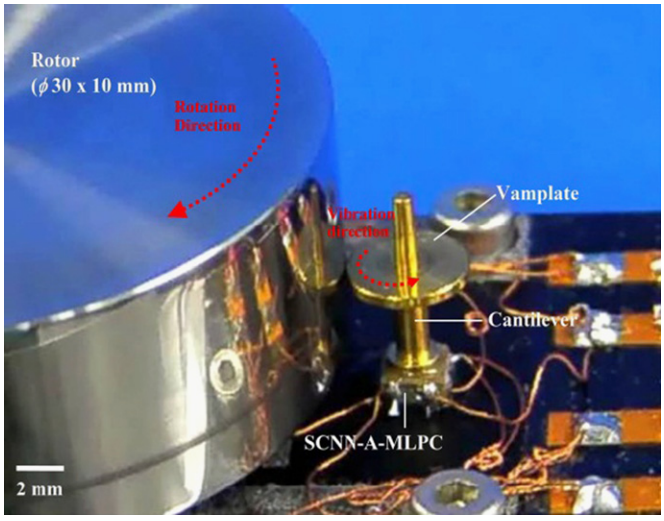

Fig. 8. Cantilever-type ultrasonic motor using SCNN–A–MLPC.

The preload was applied to the rotor from the vamplate circumference of the vibrator by pulling the base plate fixed on the vibrator.

3.2. Measurement method

The rotor was directly connected to a code wheel with 360 holes per revolution. The revolution speed was measured using a photo encoder (Avago HEDS-9100-360) that counted the number of pulses obtained by the code wheel every 20 ms. The temperature change of SCNN–A–MLPC was measured using an infrared thermometer (Horiba IT-240 S).

The motor properties were mainly evaluated by measuring the revolution speed, torque, output power density and efficiency while changing the driving voltage. At the same time, the change in the temperature of SCNN–A–MLPC was monitored. The torque was only directly calculated in the region near the maximum revolution speed and was evaluated by extrapolation using the transient response of the revolution speed in the starting period [17]. The efficiency can be obtained from the input power obtained in the stable state.

3.3. Motor properties

The motor started to rotate at the resonance frequency of the first-bending-vibration-mode rotation of 11 kHz and 6 V_{p-p}. The revolution speed increased linearly with an increase in driving voltage. Fig. 9 shows typical relationships among revolution speed, efficiency, and torque. The maximum revolution speed was about 360 rpm, and the calculated values of the maximum torque and the efficiency were about 397 μN m and 3.5%, respectively.

The relationships among output power density, the temperature change of SCNN–A–MLPC, and input power for the motor are shown in Fig. 10. The output power density increased linearly with an increase in input power.

The temperature change of SCNN–A–MLPC was almost ignorable. The average efficiency was 3.7%. The efficiency was almost the same as that of a previous study under low input power [12,13]. It was confirmed that the driving properties of the motor are maintained up to an input power of 110 mW without heat generation. In addition, the output power density of the motor is higher than that of the commercialized motor of PZT [18]. The driving properties of the motor of SCNN–A–MLPC was found to be maintained at high output power densities by reflecting the superior high-power properties of SCNN ceramics.

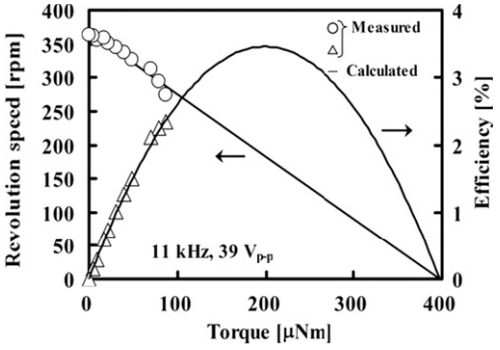

Fig. 9. Torque dependence of revolution speed and efficiency of motor.

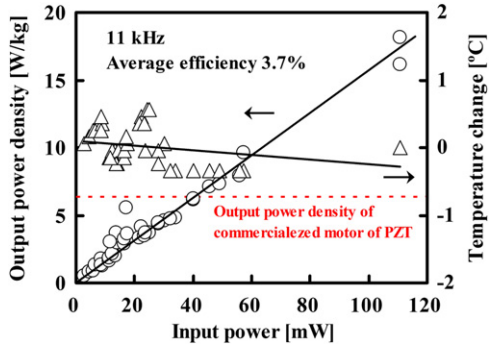

Fig. 10. Relationships among output power density, temperature change of A–MLPC, and input power for motor.

3.4. Properties of refined motor

The refined motor with build in preload mechanism was fabricated to suit the mechanical components and the driving properties were evaluated. Fig. 11 shows the refined motor. The motor was designed by the vibration analysis of stator vibrator using the finite element method (FEM) as shown in Fig. 12. The stator vibrator was oscillated at the first-bending-vibration-mode rotation of 20 kHz, where SCNN–A–MLPC was simplified to a cylinder of piezoelectric ceramics. The center shaft is not affected by vibration of vamplate in the stator vibrator. The preload between a rotor and a vamplate was applied from the shaft by a spring. The rotor can be rotated in the reverse direction with respect to the mode rotation of the stator vibrator by the friction force between the rotor bottom surface and the vamplate of the stator vibrator.

The motor properties were evaluated by measuring the revolution speeds and torque. The revolution speed was measured using a photo encoder that counted the number of pulses obtained by the code wheel. The torque was directly measured by applying the load along the circumferential direction of the rotor.

The refined motor was driven at 20 kHz of the resonance frequency of the first-bending-vibration-mode rotation. The driving properties of the motor are shown in Fig. 13. The revolution speed was 340 rpm with no load and 200 rpm with torque of 20 μN m at 2.6 V_{p-p}. The output power density was 1.4 W/kg and was lower than

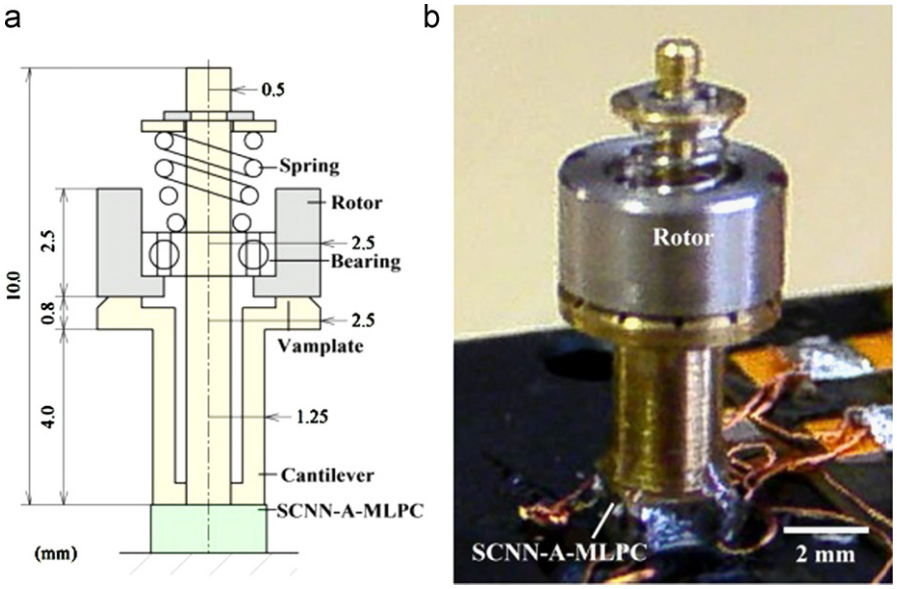

Fig. 11. Refined cantilever-type ultrasonic motor: (a) side view, and (b) picture.

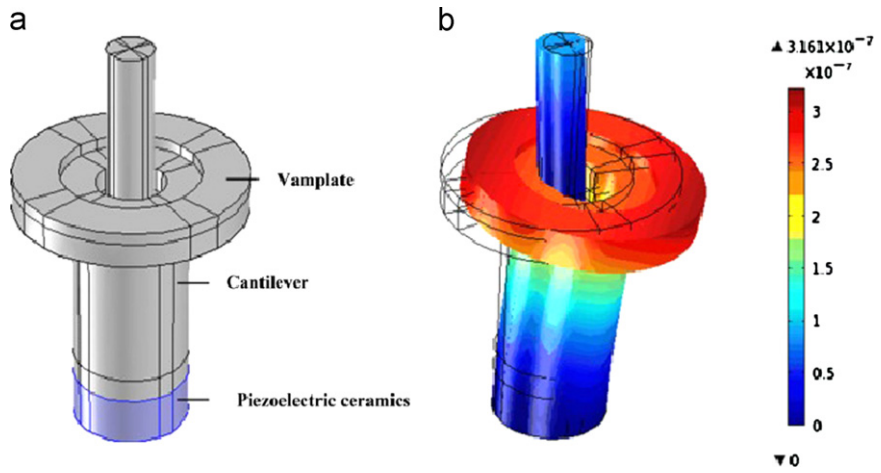

Fig. 12. Schematic views of stator vibrator using FEM: (a) simulation model, and (b) enhanced deformation shape.

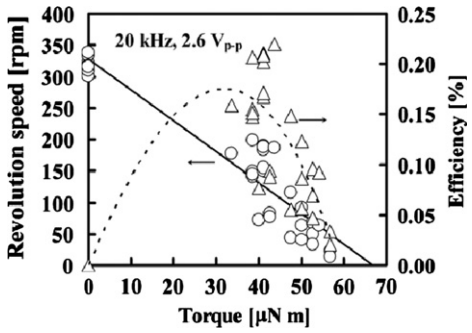

Fig. 13. Driving properties of the refined motor.

that of the motor in the former case. The difference of output power density was caused by the low efficiency of the motor, which was affected by the manufacturing and the assembly. Additional study is necessary.

4. Conclusions

We investigated the high-power properties of SCNN ceramics by comparison with them of hard PZT ceramics, and clarified the properties of the miniature cantilever-type ultrasonic motor of SCNN–A–MLPC as the lead-free-piezoelectric application.

SCNN ceramics have the nonlinear hard-spring effect in contrast to the nonlinear soft-spring effect of hard PZT ceramics and possess notable elastic properties among the piezoelectric ceramics. Under high vibration velocity, the temperature rise of SCNN ceramics was lower than that of hard PZT ceramics. Q of SCNN ceramics showed a broad peak, however Q of hard PZT ceramics drastically decreased and became lower than Q of SCNN ceramics. The degradation of Q of SCNN ceramics was thus limited, resulting in a gradual increase in the equivalent mechanical resistance. SCNN ceramics have superior high power properties than hard PZT ceramics.

The output power of the cantilever-type ultrasonic motors increased linearly with increasing input power up to 110 mW without heat generation, and the driving properties were almost the same as the expectations under low input power as previous study. The output power density of the motor was high in comparison with those of the commercialized motors of PZT ceramics.

Furthermore, the refined motor with build in preload mechanism was fabricated to suit the mechanical components. The refined motor was able to rotate with 200 rpm and 40 μN m at 2.6 V_{p-p}.

It appeared that the motors have a high potential as an environmental friendly piezoelectric device with excellent properties, reflecting the high-power properties of SCNN ceramics.

References

[1] R. Yoshida, Y. Okamoto, Micro piezoelectric actuator, Journal of the Japan Society for Precision Engineering 68 (2002) 645–648 (in Japanese).
[2] A. Iino, K. Suzuki, M. Kasuga, M. Suzuki, T. Yamanaka, Development of a self-oscillating ultrasonic micro-motor and its application to a watch, Ultrasonics 38 (2000) 54–59.
[3] S. Cagatay, B. Koc, P. Moses, K. Uchino, A piezoelectric micromotor with a stator of ϕ=1.6 mm and l=4mm using bulk PZT, Japanese Journal of Applied Physics 43 (2004) 1429–1433.
[4] H.P. Ko, K.J. Lee, K.H. Yoo, C.Y. Kang, S. Kim, S.J. Yoon, Analysis of tiny piezoelectric ultrasonic linear motor, Japanese Journal of Applied Physics 45 (2006) 4782–4786.
[5] S. Takahashi, Y. Sasaki, S. Hirose, K. Uchino, Stability of $PbZrO_3$–$PbTiO_3$–$Pb(Mn_{1/3}Sb_{2/3})O_3$ piezoelectric ceramics under vibration-level change, Japanese Journal of Applied Physics 34 (1995) 5328–5331.
[6] S. Kawada, H. Ogawa, M. Kimura, K. Shiratsuyu, Y. Higuchi, Relationship between vibration direction and high-power characteristics of <001>-textured $SrBi_2Nb_2O_9$ ceramics, Japanese Journal of Applied Physics 46 (2007) 7079–7083.
[7] Y. Noumura, Y. Hiruma, H. Nagata, T. Takenaka, High-power piezoelectric characteristics of $Bi_4Ti_3O_{12}$–$SrBi_4Ti_4O_{15}$-based ferroelectric ceramics, Japanese Journal of Applied Physics 50 (2011) 07HB06.
[8] D. Tanaka, J. Yamazaki, M. Furukawa, T. Tsukada, High power characteristics of $(Ca,Ba)TiO_3$ piezoelectric ceramics with high mechanical quality factor, Japanese Journal of Applied Physics 49 (2010) 09MD03.
[9] Y. Doshida, H. Shimizu, Y. Mizuno, K. Itoh, S. Hirose, H. Tamura, Nonlinear behavior and high-power properties of $(Bi,Na,Ba)TiO_3$

and $(Sr,Ca)_2NaNb_5O_{15}$piezoelectric ceramics, Japanese Journal of Applied Physics 50 (2011) 09ND06.

[10] T. Tou, Y. Hamaguti, Y. Maida, H. Yamamori, K. Takahashi, Y. Terashima, Properties of $(Bi_{0.5}Na_{0.5})TiO_3$–$BaTiO_3$–$(Bi_{0.5}Na_{0.5})$-$(Mn_{1/3}Nb_{2/3})O_3$ lead-free piezoelectric ceramics and its application to ultrasonic cleaner, Japanese Journal of Applied Physics 48 (2009) 07GM03.

[11] Y. Doshida, S. Kishimoto, K. Ishii, H. Kishi, H. Tamura, Y. Tomikawa, S. Hirose, Miniature cantilever-type ultrasonic motor using Pb-free multilayer piezoelectric ceramics, Japanese Journal of Applied Physics 46 (2007) 4921–4925.

[12] Y. Doshida, S. Kishimoto, T. Irieda, H. Tamura, Y. Tomikawa, S. Hirose, Double-mode miniature cantilever-type ultrasonic motor using lead-free array-type multilayer piezoelectric ceramics, Japanese Journal of Applied Physics 47 (2008) 4242–4247.

[13] Y. Doshida, H. Shimizu, T. Irieda, H. Tamura, Y. Tomikawa, S. Hirose, Investigation of miniature cantilever-type ultrasonic motor using lead-free array-type multilayer piezoelectric ceramics, Japanese Journal of Applied Physics 49 (2010) 07HE25.

[14] E. Li, R. Sasaki, T. Hoshina, H. Takeda, T. Tsurumi, Miniature ultrasonic motor using shear mode of potassium sodium niobate-based lead-free piezoelectric ceramics, Japanese Journal of Applied Physics 48 (2009) 09KD11.

[15] H. Tamura, K. Itoh, Y. Doshida, Y. Yamayoshi, S. Hirose, Software-controlled measurement system for large vibrational amplitude piezoelectric resonator using continuous driving method with numerical equivalent model, Japanese Journal of Applied Physics 50 (2011) 07HC11.

[16] S.O. Ural, S. Tuncdemir, Y. Zhuang, K. Uchino, Development of a high power piezoelectric characterization system and its application for resonance/antiresonance mode characterization, Japanese Journal of Applied Physics 48 (2009) 056509.

[17] K. Nakamura, M. Kurosawa, H. Kurebayashi, S. Ueha, An estimation of load characteristics of an ultrasonic motor by measuring transient responses, IEEE Transactions on Ultrasonics, Ferroelectrics and Frequency Control 38 (1991) 481–485.

[18] S. Ueha, Y. Tomikawa, Ultrasonic Motors Theory and Applications, Clarendon Press, Oxford and New York, 1993, p. 199.